Table 1. Demographic and clinical characteristics of the patients with schizophrenia

Subject	Age (yr), sex	PANSS				Duration of illness (yr)	Duration of drug treatment (yr)	Haloperidol equivalent (mg)	Main antipsychotics
		Positive	Negative	General	Total				
1	29, F	12	12	25	49	11	9	3	Olanzapine
2	34, F	17	12	33	62	7	5	6	Risperidone
3	37, F	14	23	27	64	0.5	0.5	3	Olanzapine
4	43, F	21	27	49	97	22	19	17	Risperidone
5	46, F	16	15	34	65	33	21	10	Nemonapride
6	49, F	24	20	33	77	23	16	19.4	Haloperidol
7	42, M	15	22	27	64	4	4	4	Olanzapine
8	43, M	15	26	33	74	26	23	9	Haloperidol
9	44, M	22	25	40	87	22	22	8.5	Olanzapine
10	44, M	16	26	37	79	4	4	14	Haloperidol
11	46, M	29	26	56	111	26	26	3.5	Olanzapine
12	46, M	16	16	25	57	24	24	4	Risperidone
13	52, M	24	35	58	117	18	17	16.5	Olanzapine
14	59, M	27	24	47	87	43	39	10.3	Mosapramine
		19.1 ± 5.3	22.1 ± 6.5	37.4 ± 11.1	77.9 ± 20.1	18.8 ± 12.2	16.4 ± 10.8	9.2 ± 5.7	

PANSS, Positive and Negative Syndrome Scale; F, female; M, male.
Haloperidol (1 mg) was equivalent to chlorpromazine (50 mg).

demonstrated to be useful in the study of neuro-degerative disorders such as Alzheimer's disease (Yasuno et al. 2008).

In this study, we investigated PBR binding in patients with chronic schizophrenia using [^{11}C]DAA1106 to evaluate whether glial reaction was involved in the pathophysiology of schizophrenia.

Materials and methods

Subjects

Fourteen patients with schizophrenia [six females, eight males; 43.9 ± 7.4 yr (mean $\pm$ s.d.)] and 14 normal control subjects (five females, nine males; 42.5 ± 9.0 yr) were enrolled in this study. Patients were recruited from the outpatient and in-patient units of Nippon Medical School Hospital, Asai Hospital and Sobu Hospital, located in Tokyo and Chiba prefecture in Japan. The patients were diagnosed as having schizophrenia and treated by attending physicians at each hospital, and their diagnoses were re-evaluated with structured interviews at our PET centre. All 14 patients were diagnosed with schizophrenia according to DSM-IV criteria. Exclusion criteria were current or past substance, cannabis or alcohol abuse, mood disorders, and organic brain disease. The patients' demographic and clinical data are shown in Table 1. None of the patients had taken benzodiazepines within more than 1 month prior to PET measurements.

Psychopathology was assessed by the Positive and Negative Syndrome Scale (PANSS; Kay et al. 1987). PANSS was completed by three experienced psychiatrists on the same day as the PET measurements. They reviewed the ratings after the interviews, and disagreements were resolved by consensus; the consensus ratings were used in this study. The symptom scores were calculated as total scores, positive symptom, negative symptom, and general symptom subscores of PANSS. The total PANSS score ranged from 49 to 117 (78.6 ± 20.7). The mean positive symptom score was 19.1 ± 5.3, negative symptom score was 22.1 ± 6.5, and general symptom score was 37.4 ± 11.1.

The normal control subjects were recruited from the surrounding community. Based on psychiatric screening interviews, they were free of current and past psychiatric or major medical disease, and had no relatives with neuropsychiatric disorders.

This study complied with the current laws of Japan, and was approved by the Ethics and Radiation Safety Committee of the National Institute of Radiological Sciences, Chiba, Japan. Written informed consent was obtained from all subjects.

Radiochemistry

[^{11}C]DAA1106 was prepared as described in detail previously (Ikoma et al. 2007; Zhang et al. 2003). The precursor was supplied by Taisho Pharmaceutical Co. (Japan).

PET data acquisition

PET scans were performed with ECAT EXACT HR+ (CTI-Siemens, USA), which provides 63 planes and a 15.5-cm axial field of view (FOV). A 10-min transmission scan with a ^{68}Ge–^{68}Ga source was followed by a 90-min dynamic scan (20s × 9, 60s × 5, 120s × 4, 240s × 11, and 300s × 6) with a bolus injection of 261–411 (369 ± 27) MBq of [^{11}C]DAA1106. Specific radioactivity was 15.4–220.7 GBq/μmol at the time of the injection. There was no significant difference in injected radioactivity and specific radioactivity between patients and normal controls (373 ± 20 MBq and 60.3 ± 44.4 GBq/μmol for patients, and 366 ± 32 MBq and 98.4 ± 70.7 GBq/μmol for normal controls). Radioactivity was measured in three-dimensional mode, and the data were reconstructed with a Hanning filter with a cut-off frequency of 0.4 (full width half maximum = 7.5 mm).

Arterial blood sampling

To obtain the arterial input function, an automated blood sampling system was used for continuous (counts/s) blood radioactivity measurements during the first 12 min of PET measurement. At the same time, arterial blood samples were taken manually and their radioactivity concentration was measured 13 times during the initial 3 min after the injection, eight times during the next 17 min, and once every 10 min until the end of the scan. To analyse the metabolite fraction in the plasma, arterial blood samples were taken 10 times during PET measurements. The parent ligand, separated from the total radioactive compound, was measured as previously described (Ikoma et al. 2007). The mean time-course of the fraction of the parent ligand is shown in Fig. 1. There was a significant group × time interaction using repeated-measures ANOVA with Greenhouse–Geisser correction ($F_{3.4,81.1}$ = 4.92, p = 0.002), although one subject from each group was excluded for the statistical analysis due to one missing data-point.

MR imaging

T1-weighted magnetic resonance imaging (MRI) of the brain was performed with Philips Intera 1.5 T (Philips Medical Systems, The Netherlands). T1-weighted images of the brain were obtained from all subjects. The scan parameters were 1-mm-thick 3D T1 images with a transverse plane [repetition time (TR)/echo time (TE) 22/9.2 ms, flip angle 30′, matrix 128 × 128, FOV 256 × 256). Voxel size of the magnetic resonance images was 1 mm × 1 mm × 1 mm.
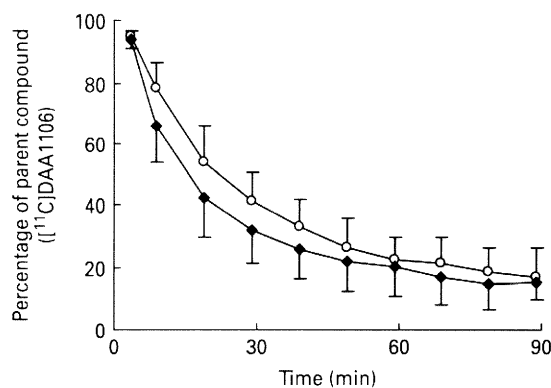

Fig. 1. Mean time-course of the percentage of parent compound ([^{11}C]DAA1106) after venous injection of [^{11}C]DAA1106 between normal controls (–○–) and patients (–◆–) with schizophrenia.

Data analysis

Eleven regions of interest (ROIs) (medial frontal cortex, dorsolateral frontal cortex, medial temporal cortex, lateral temporal cortex, parietal cortex, occipital cortex, thalamus, striatum, cerebellum, anterior cingulate cortex, and posterior cingulate cortex) were delineated on the co-registered PET/MRI images. In addition to each regional ROI, eight cortical ROIs (medial frontal cortex, dorsolateral frontal cortex, medial temporal cortex, lateral temporal cortex, parietal cortex, occipital cortex, anterior cingulate cortex, and posterior cingulate cortex) were also summed up as total cortical regions.

Regional time–activity data were analysed with two-tissue compartment model (2-TC) with the metabolite-corrected plasma input function, a model demonstrated to estimate binding potential (BP$_{ND}$) most reliably for [^{11}C]DAA1106 (Ikoma et al. 2007). Rate constants were estimated with weighted least squares and the Marquardt optimizer. For each region, k_1, k_2, k_3, k_4 and blood volume were estimated by 2-TC. BP$_{ND}$ was calculated as k_3/k_4 in this analysis. Data analysis was performed with PMOD 2.65 (PMOD Technologies, Switzerland).

Statistical analysis

Regional ROIs

Statistical analysis of the difference of regional BP$_{ND}$ for each ROI (for total 11 ROIs) between patients and normal controls was performed by repeated-measures ANOVA ($p < 0.05$ was considered significant). When any interaction was found, post-hoc Bonferroni correction was used for multiple comparisons.

Table 2. Significant correlation between PANSS scores and regional [^{11}C]DAA1106 binding

PANSS scores	Region	p value
Positive symptom	Medial frontal cortex	0.002*
	Dorsolateral frontal cortex	0.022
	Medial temporal cortex	0.003*
	Lateral temporal cortex	0.013
	Parietal cortex	0.005
	Occipital cortex	0.001*
	Cerebellum	0.022
	Striatum	0.010
Negative symptom	None	
General symptom	Medial frontal cortex	0.018
	Medial temporal cortex	0.027
	Occipital cortex	0.038
Total score	Medial frontal cortex	0.012
	Medial temporal cortex	0.029
	Parietal cortex	0.044
	Occipital cortex	0.017

PANSS, Positive and Negative Syndrome Scale.
* $p < 0.0045$ (0.05/11).

Fig. 2. Positive correlation between [^{11}C]DAA1106 BP_{ND} in the occipital cortex and positive symptom scores in the Positive and Negative Syndrome Scale.

Correlation between regional BP_{ND} values and PANSS scores were analysed with Pearson's correlation method ($p < 0.05$ was considered significant).

Correlation between regional BP_{ND} values and duration of illness, duration of drug treatment, and chlorpromazine equivalent doses (Inagaki et al. 1999) were analysed with Pearson's correlation method ($p < 0.05$ was considered significant).
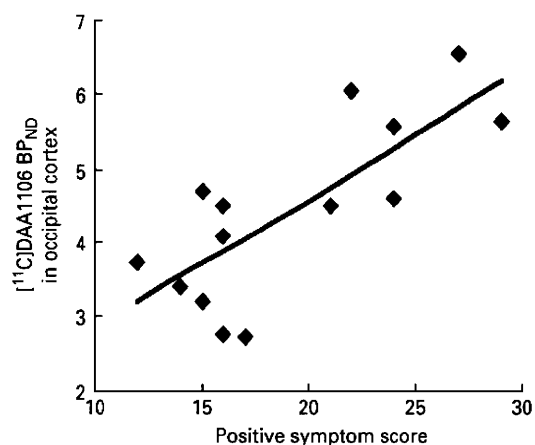
Changes in regional BP_{ND} values with age were analysed with Pearson's correlation method for patients and normal controls, respectively ($p < 0.05$ was considered significant).

Total cortical regions

For analysing differences in total cortical regions between patients and normal controls, Student's t test was used ($p < 0.05$ was considered significant).

Correlations between BP_{ND} values in total cortical regions and PANSS scores were analysed with Pearson's correlation method ($p < 0.05$ was considered significant).

Correlation between BP_{ND} values in total cortical regions and duration of illness, duration of drug treatment, and chlorpromazine-equivalent doses (Inagaki et al. 1999) were analysed with Pearson's correlation method ($p < 0.05$ was considered significant).

Changes in BP_{ND} values in total cortical regions with age were analysed with Pearson's correlation method for patients and normal controls, respectively ($p < 0.05$ was considered significant).

Results

Regional ROIs

Comparison of regional BP_{ND} values for [^{11}C]DAA1106 between the patients with schizophrenia and normal controls by two-way repeated ANOVA with Greenhouse–Geisser correction showed no significant group × region interaction ($F_{1.7,44.4} = 0.542, p = 0.558$).

For the correlation analysis between BP_{ND} values in regional ROIs and positive symptom scores in the patient group, significant correlations were found in regions such as the medial frontal cortex, medial temporal cortex and occipital cortex (Table 2) (Fig. 2). No correlation was found between BP_{ND} values of each region and negative symptoms. Those three regions showed trends of positive correlation with general symptoms and total score (Table 2). There was no significant correlation between regional BP_{ND} and the duration of illness.

There was no significant change of regional BP_{ND} values with age in normal controls, whereas significant changes in BP_{ND} values with age in the patients with schizophrenia were observed in the occipital cortex ($p = 0.014$), lateral temporal cortex ($p = 0.023$), parietal cortex ($p = 0.023$), medial temporal cortex ($p = 0.031$), and medial frontal cortex ($p = 0.036$).
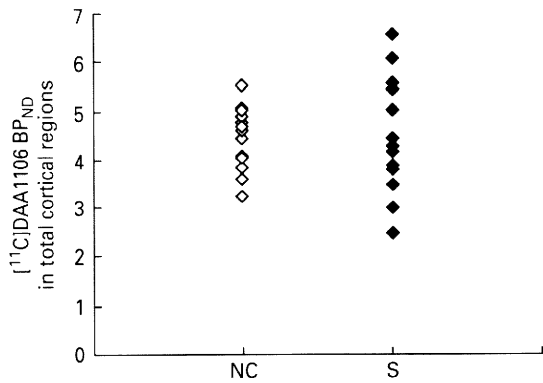
Fig. 3. Comparison of [^{11}C]DAA1106 BP$_{ND}$ of total cortical regions between normal controls (NC) and patients with schizophrenia (S).

Fig. 4. Positive correlation between [^{11}C]DAA1106 BP$_{ND}$ in the total cortical region and positive symptom scores in the Positive and Negative Syndrome Scale.

Fig. 5. Positive correlation between [^{11}C]DAA1106 BP$_{ND}$ in the total cortical region and duration of illness.

Total cortical regions

There was no significant difference of BP$_{ND}$ values in total cortical regions between patients with schizophrenia and normal controls (Fig. 3). Significant correlation was found with the positive symptom scores ($p = 0.006$) (Fig. 4). There was no significant correlation with other symptom scores (negative, general, and total symptom scores). Total cortical regions were correlated with duration of illness ($p = 0.020$) (Fig. 5) and duration of drug treatment ($p = 0.023$). BP$_{ND}$ of total cortical regions was not correlated with chlorpromazine-equivalent doses.

There was no significant change of BP$_{ND}$ values in total cortical regions with age in normal controls, but significant changes of BP$_{ND}$ values with age were observed in total cortical regions of the patients with schizophrenia ($p = 0.018$).

Discussion

In this study, [^{11}C]DAA1106 binding, which was considered to correspond to the density of PBR, was not different between the patients with chronic schizophrenia and normal controls. A recent study demonstrated that [^{11}C]PK11195 binding increased in total grey matter in patients with acute-onset schizophrenia (van Berckel et al. 2008). Another recent study reported that [^{11}C]PK11195 binding in the hippocampus was significantly increased in patients with schizophrenia during acute psychosis, while there was no significant difference in other regions compared with normal controls (Doorduin et al. 2009). To understand the difference in the results between the present study and the two [^{11}C]PK11195 studies, several factors, such as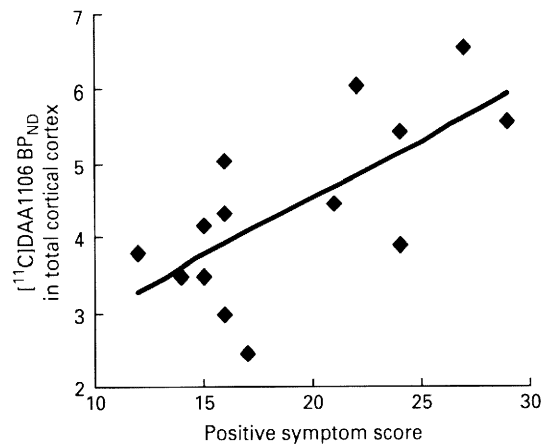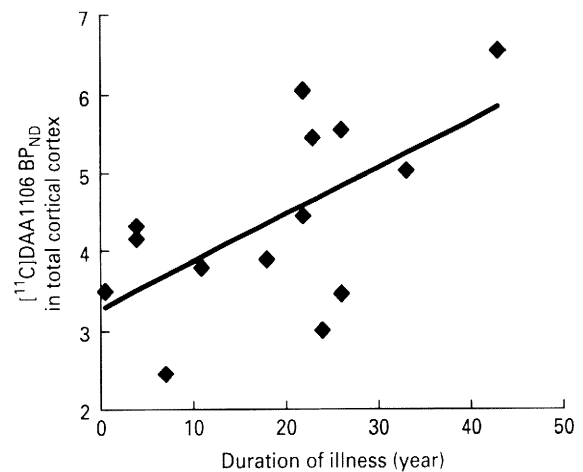 the use of different radioligands and different patient groups, should be taken into consideration. Although PK11195 fully displaced the [^{3}H]DAA1106 binding (Chaki et al. 1999), a high concentration of PK11195 was required for this displacement. This suggested that the binding domain for DAA1106 contains an extra component that does not interact efficiently with PK11195 (Chaki et al. 1999). The mean age of patients with schizophrenia enrolled in the present study was higher (44 yr in 14 patients) than those in the two [^{11}C]PK11195 studies (24 yr in 10 patients, and 31 yr in seven patients). Most of the patients in the present study were at the chronic stage.

Within the patient group, [^{11}C]DAA1106 binding had a significant correlation with the positive symptom score of PANSS, a finding that might be in line

with those recent findings with [^{11}C]PK11195. The present results might indicate that the activated neuro-immune system was related to the pathophysiology of schizophrenia at the chronic stage.

In previous MRI volumetric research in schizophrenia, volume reduction in the brain has been reported in patients with chronic schizophrenia (Shenton *et al.* 2001). However, in the present study, there was no significant difference in the volume of ROIs by ANOVA, and total cortical ROI by Student's *t* test between the patients and normal controls (data not shown). Thus, the insignificance of the difference of [^{11}C]DAA1106 binding between the patients and normal controls is not related to the partial volume effect due to brain atrophy.

In this study, normal controls showed no age effects on [^{11}C]DAA1106 binding in any region. This is in line with the report with [^{11}C]PK11195 binding except the thalamus, where [^{11}C]PK11195 binding was reported to increase with age (Cagnin *et al.* 2001). This might be due to different radioligands or different age ranges between the two studies (24–55 yr in this study and 32–80 yr in the [^{11}C]PK11195 study). On the other hand, [^{11}C]DAA1106 binding was found to increase with age in patients with schizophrenia. Schizophrenia has been considered to be progressive in functional disability and morphological changes (Lieberman *et al.* 2001; Mathalon *et al.* 2001; Saijo *et al.* 2001). The present results of the positive correlation among [^{11}C]DAA1106 binding, duration of illness, and age might suggest that the progressive change occurs at the glial reaction level.

A recent meta-analysis showed that some cytokines such as IL-1RA, sIL-2R, and IL-6 are increased in schizophrenia (Potvin *et al.* 2008). PBR has been considered to modulate the release of pro-inflammatory cytokines in the CNS. PBR was reported to modulate the release of the inflammatory molecules NO and tumour necrosis factor-alpha (TNF-α) (Wilms *et al.* 2003). A PBR ligand, PK11195, has been reported to inhibit lipopolysaccharide-induced expressions of COX-2 and TNF-α in human microglia (Choi *et al.* 2002). Immunomodulatory drugs such as cyclooxygenase-2 (COX-2) inihibitors have been reported to show beneficial effects in schizophrenia (Muller & Schwarz, 2008). The combination of risperidone and COX-2 inhibitor has been reported to show superiority over risperidone alone in positive symptoms and PANSS total scores (Akhondzadeh *et al.* 2007). On the other hand, cytokines such as IL-2 and IL-6 are reported to increase after olanzapine and clozapine treatment (Kluge *et al.* 2009). The present results of PBR binding in the patients with schizophrenia might be in accord with the previous reports of cytokines.

A recent report demonstrated that PBR expression was not confined to microglia but was inducible in nervous tissue cells of neuroepithelial origin (Ji *et al.* 2008). Thus, PBR binding might also arise from astrocytes and other non-microglial elements. Schizophrenia patients with high S100B serum concentration, considered to indicate astrocyte activation, were reported to have cognitive dysfunction compared with patients with low S100B serum concentration (Pedersen *et al.* 2008). DAA1106 binding in patients with schizophrenia might also be related to the change in PBR on astrocytes.

In a post-mortem study, a subgroup of the patients with schizophrenia who committed suicide had increased microglial densities, although microglial HLA-DR expression in the patients with schizophrenia was not different from normal controls (Steiner *et al.* 2008). Microglial activation has been suggested to be interpretable as a consequence of pre-suicidal stress (Avital *et al.* 2001; Lehmann *et al.* 2002).

Although BP$_{ND}$ of total cortical regions was not correlated with chlorpromazine-equivalent doses in the present study, some antipsychotics were reported to have anti-inflammatory effects (Kato *et al.* 2007; Kowalski *et al.* 2003, 2004; Labuzek *et al.* 2005; Zheng *et al.* 2008). The effect of antipsychotics on DAA1106 binding remains to be studied.

There are several confounding factors in the present study. First, the number of subjects was relatively small. Further larger-scale studies will be needed to confirm the present results. Second, all the patients were under different kinds of antipsychotic treatment. Further study is needed with drug-naive patients and patients under well-controlled drug treatment. Third, the PANSS scores of patients were higher as the duration of the illness was longer and age increased. This might reflect a possible subgroup of treatment-resistant patients.

In conclusion, we found no significant differences in PBR binding between the brains of patients with schizophrenia and those of normal control subjects, unlike recent reports with [^{11}C]PK11195 (van Berckel *et al.* 2008; Doorduin *et al.* 2009). Nevertheless, PBR binding in the patients with schizophrenia was correlated with positive symptoms, disease duration and age. The present results suggest that the glial reaction process might be involved in the pathophysiology of schizophrenia. Although the correlations should be interpreted with caution, these results at least suggest that additional studies are warranted in order to determine whether baseline

differences exist between patients with schizophrenia and healthy subjects, as well as to reveal the biological meanings of the correlations with disease parameters.

Acknowledgments

Statement of Interest

None.

References

Akhondzadeh S, Tabatabaee M, Amini H, Ahmadi Abhari SA, *et al.* (2007). Celecoxib as adjunctive therapy in schizophrenia: a double-blind, randomized and placebo-controlled trial. *Schizophrenia Research* **90**, 179–185.

Avital A, Richter-Levin G, Leschiner S, Spanier I, *et al.* (2001). Acute and repeated swim stress effects on peripheral benzodiazepine receptors in the rat hippocampus, adrenal, and kidney. *Neuropsychopharmacology* **25**, 669–678.

Cagnin A, Brooks DJ, Kennedy AM, Gunn RN, *et al.* (2001). In-vivo measurement of activated microglia in dementia. *Lancet* **358**, 461–467.

Chaki S, Funakoshi T, Yoshikawa R, Okuyama S, *et al.* (1999). Binding characteristics of [^{3}H]DAA1106, a novel and selective ligand for peripheral benzodiazepine receptors. *European Journal of Pharmacology* **371**, 197–204.

Choi HB, Khoo C, Ryu JK, van Breemen E, *et al.* (2002). Inhibition of lipopolysaccharide-induced cyclooxygenase-2, tumor necrosis factor-alpha and [Ca^{2+}]$_i$ responses in human microglia by the peripheral benzodiazepine receptor ligand pK11195. *Journal of Neurochemistry* **83**, 546–555.

Doorduin J, de Vries EF, Willemsen AT, de Groot JC, *et al.* (2009). Neuroinflammation in schizophrenia-related psychosis: a pET study. *Journal of Nuclear Medicine* **50**, 1801–1807.

Ikoma Y, Yasuno F, Ito H, Suhara T, *et al.* (2007). Quantitative analysis for estimating binding potential of the peripheral benzodiazepine receptor with [^{11}C]DAA1106. *Journal of Cerebral Blood Flow and Metabolism* **27**, 173–184.

Inagaki A, Inada T, Fujii Y, Gohei Y, *et al.* (1999). *Equivalent Doses of Antipsychotic Medications* [in Japanese]. Tokyo: Seiwa Press.

Jakubikova J, Duraj J, Hunakova L, Chorvath B, *et al.* (2002). PK11195, an isoquinoline carboxamide ligand of the mitochondrial benzodiazepine receptor, increased drug uptake and facilitated drug-induced apoptosis in human multidrug-resistant leukemia cells in vitro. *Neoplasma* **49**, 231–236.

Ji B, Maeda J, Sawada M, Ono M, *et al.* (2008). Imaging of peripheral benzodiazepine receptor expression as biomarkers of detrimental *vs.* beneficial glial responses in mouse models of alzheimer's and other cNS pathologies. *Journal of Neuroscience* **28**, 12255–12267.

Kato T, Monji A, Hashioka S, Kanba S (2007). Risperidone significantly inhibits interferon-gamma-induced microglial activation in vitro. *Schizophrenia Research* **92**, 108–115.

Kay SR, Fiszbein A, Opler LA (1987). The positive and negative syndrome scale (PANSS) for schizophrenia. *Schizophrenia Bulletin* **13**, 261–276.

Kluge M, Schuld A, Schacht A, Himmerich H, *et al.* (2009). Effects of clozapine and olanzapine on cytokine systems are closely linked to weight gain and drug-induced fever. *Psychoneuroendocrinology* **34**, 118–128.

Kowalski J, Labuzek K, Herman ZS (2003). Flupentixol and trifluperidol reduce secretion of tumor necrosis factor-alpha and nitric oxide by rat microglial cells. *Neurochemistry International* **43**, 173–178.

Kowalski J, Labuzek K, Herman ZS (2004). Flupentixol and trifluperidol reduce interleukin-1 beta and interleukin-2 release by rat mixed glial and microglial cell cultures. *Polish Journal of Pharmacology* **56**, 563–570.

Labuzek K, Kowalski J, Gabryel B, Herman ZS (2005). Chlorpromazine and loxapine reduce interleukin-1beta and interleukin-2 release by rat mixed glial and microglial cell cultures. *European Neuropsychopharmacology* **15**, 23–30.

Lehmann J, Weizman R, Leschiner S, Feldon J, *et al.* (2002). Peripheral benzodiazepine receptors reflect trait (early handling) but not state (avoidance learning). *Pharmacology Biochemistry and Behavior* **73**, 87–93.

Lieberman J, Chakos M, Wu H, Alvir J, *et al.* (2001). Longitudinal study of brain morphology in first episode schizophrenia. *Biological Psychiatry* **49**, 487–499.

Lin A, Kenis G, Bignotti S, Tura GJ, *et al.* (1998). The inflammatory response system in treatment-resistant schizophrenia: increased serum interleukin-6. *Schizophrenia Research* **32**, 9–15.

Maeda J, Suhara T, Zhang MR, Okauchi T, *et al.* (2004). Novel peripheral benzodiazepine receptor ligand [11C]DAA1106 for pET: an imaging tool for glial cells in the brain. *Synapse* **52**, 283–291.

Mathalon DH, Sullivan EV, Lim KO, Pfefferbaum A (2001). Progressive brain volume changes and the clinical course of schizophrenia in men: a longitudinal magnetic resonance imaging study. *Archives of Genenal Psychiatry* **58**, 148–157.

Muller N, Schwarz MJ (2008). COX-2 inhibition in schizophrenia and major depression. *Current Pharmaceutical Design* **14**, 1452–1465.

Nawa H, Takei N (2006). Recent progress in animal modeling of immune inflammatory processes in schizophrenia: implication of specific cytokines. *Neuroscience Research* **56**, 2–13.

Okuyama S, Chaki S, Yoshikawa R, Ogawa S, et al. (1999). Neuropharmacological profile of peripheral benzodiazepine receptor agonists, dAA1097 and dAA1106. *Life Science* **64**, 1455–1464.

Pedersen A, Diedrich M, Kaestner F, Koelkebeck K, *et al.* (2008). Memory impairment correlates with increased s100B serum concentrations in patients with chronic schizophrenia. *Progress in Neuro-psychopharmacology and Biological Psychiatry* **32**, 1789–1792.

Potvin S, Stip E, Sepehry AA, Gendron A, et al. (2008). Inflammatory cytokine alterations in schizophrenia: a systematic quantitative review. *Biological Psychiatry* **63**, 801–808.

Saijo T, Abe T, Someya Y, Sassa T, et al. (2001). Ten year progressive ventricular enlargement in schizophrenia: an mRI morphometrical study. *Psychiatry and Clinical Neuroscience* **55**, 41–47.

Shah F, Hume SP, Pike VW, Ashworth S, et al. (1994). Synthesis of the enantiomers of [N-methyl-^{11}C]PK 11195 and comparison of their behaviours as radioligands for pK binding sites in rats. *Nuclear Medicine and Biology* **21**, 573–581.

Shenton ME, Dickey CC, Frumin M, McCarley RW (2001). A review of mRI findings in schizophrenia. *Schizophrenia Research* **49**, 1–52.

Steiner J, Bielau H, Brisch R, Danos P, et al. (2008). Immunological aspects in the neurobiology of suicide: elevated microglial density in schizophrenia and depression is associated with suicide. *Journal of Psychiatric Research* **42**, 151–157.

Vaalburg W, Hendrikse NH, Elsinga PH, Bart J, et al. (2005). P-glycoprotein activity and biological response. *Toxicology and Applied Pharmacology* **207**, 257–260.

van Berckel BN, Bossong MG, Boellaard R, Kloet R, et al. (2008). Microglia activation in recent-onset schizophrenia: a quantitative (R)-[^{11}C]PK11195 positron emission tomography study. *Biological Psychiatry* **64**, 820–822.

Wilms H, Claasen J, Rohl C, Sievers J, et al. (2003). Involvement of benzodiazepine receptors in neuroinflammatory and neurodegenerative diseases: evidence from activated microglial cells in vitro. *Neurobiology of Disease* **14**, 417–424.

Yasuno F, Ota M, Kosaka J, Ito H, et al. (2008). Increased binding of peripheral benzodiazepine receptor in alzheimer's disease measured by positron emission tomography with [^{11}C]DAA1106. *Biological Psychiatry* **64**, 835–841.

Zhang MR, Kida T, Noguchi J, Furutsuka K, et al. (2003). [^{11}C]DAA1106: radiosynthesis and in vivo binding to peripheral benzodiazepine receptors in mouse brain. *Nuclear Medicine and Biology* **30**, 513–519.

Zhang XY, Zhou DF, Cao LY, Zhang PY, et al. (2004). Changes in serum interleukin-2, -6, and -8 levels before and during treatment with risperidone and haloperidol: relationship to outcome in schizophrenia. *Journal of Clinical Psychiatry* **65**, 940–947.

Zheng LT, Hwang J, Ock J, Lee MG, et al. (2008). The antipsychotic spiperone attenuates inflammatory response in cultured microglia via the reduction of proinflammatory cytokine expression and nitric oxide production. *Journal of Neurochemistry* **107**, 1225–1235.

ORIGINAL ARTICLE

Quantitative analysis of dopamine transporters in human brain using [11C]PE2I and positron emission tomography: evaluation of reference tissue models

Chie Seki · Hiroshi Ito · Tetsuya Ichimiya · Ryosuke Arakawa · Yoko Ikoma ·
Miho Shidahara · Jun Maeda · Akihiro Takano · Hidehiko Takahashi ·
Yuichi Kimura · Kazutoshi Suzuki · Iwao Kanno · Tetsuya Suhara

Abstract

Objective Dopamine transporter (DAT) is a reuptake carrier of dopamine at presynapse that regulates dopaminergic neural transmission. [11C]PE2I is a cocaine analog developed as a potent positron emission tomography (PET) ligand for DAT with high selectivity. The aim of this study was to evaluate the applicability of quantification methods using reference tissue models for [11C]PE2I.

Methods Dynamic PET scans were performed in 6 young healthy male volunteers after an intravenous bolus injection of [11C]PE2I. Metabolite-corrected arterial plasma-input functions were obtained. Compartment model analysis and plasma-input Logan analysis were performed to determine the kinetic parameters and distribution volume (V_T). The distribution volume ratio (*DVR*) was calculated as the ratio of V_T in the cerebral region to that in the cerebellum. *DVR*s were also determined by the original multilinear reference tissue model method (MRTMo) and the simplified reference tissue model method (SRTM), comparing the results with those obtained from graphical analysis using arterial input function. To estimate errors in *DVR* calculated using the reference tissue model, a simulation study that focused on cerebellar kinetics and scan duration was performed.

Results The highest [11C]PE2I binding was observed in the striatum, followed by the midbrain and thalamus. The 2-tissue model was preferable to the 1-tissue model for describing the [11C]PE2I kinetics in the cerebellum. Both the measured and 90-min simulated data showed that reference tissue models caused an underestimation of *DVR* in the striatum. The simulation showed that 90-min scan duration was insufficient when cerebellar kinetics was described as a 1-tissue model. Nevertheless, *DVR* values determined by MRTMo and SRTM were in good agreement with those by the graphical approach in other lower binding regions.

Conclusion Due to the [11C]PE2I kinetics in the cerebellum and limited scan duration for 11C, MRTMo and SRTM underestimated the striatal *DVR*. Despite this limitation, the present study demonstrated the applicability of reference tissue models. Since DAT in the midbrain and thalamus is of interest in the pathophysiology of neuropsychiatric disease, this noninvasive quantitative analysis will be useful for clinical investigations.

Keywords [11C]PE2I · Human · Kinetic modeling · Positron emission tomography (PET) · Reference tissue model

Introduction

Dopaminergic neurotransmission is of interest in the pathophysiology of neuropsychiatric disease. One of the presynaptic functions is the dopamine reuptake mediated by dopamine transporter (DAT), a membrane-bound protein. A number of radioligands for in vivo DAT imaging have been developed for positron emission tomography (PET), such as [11C]cocaine [1], [11C]WIN35,428 (CFT) [2, 3], [11C]β-CIT (RTI-55) [4], [11C] β-CIT-FE [5], [11C]D-threo-methylphenidate [6], [18F]FECNT [7], [11C]Altropane [8], [11C]PE2I [9] and most recently [11C]LBT-999 [10]. Most of them are analogs of cocaine

C. Seki · H. Ito (✉) · T. Ichimiya · R. Arakawa · Y. Ikoma ·
M. Shidahara · J. Maeda · A. Takano · H. Takahashi ·
Y. Kimura · K. Suzuki · I. Kanno · T. Suhara
Molecular Imaging Center, National Institute of Radiological
Sciences, 4-9-1 Anagawa, Inage-ku, Chiba 263-8555, Japan
e-mail: hito@nirs.go.jp

🖄 Springer

and have some degree of affinity for the serotonin transporter. The tropane analog N-(3-iodoprop-2E-enyl)-2β-carbomethoxy-3β-(4-methylphenyl) nortropane (PE2I) has 29-fold higher affinity for DAT than for serotonin transporter and more than 58-fold higher affinity than for noradrenalin transporter [9]. Thus, ^{11}C-labeled PE2I, [^{11}C]PE2I(([^{11}C]-(E)-N-3-isodoprop-2-ethyl)-2β-carbomethoxy-3β-(4-methylphenyl)nortropane), can be expected to represent a selective PET radioligand for the evaluation of DAT.

Previous reports have demonstrated the successful visualization of brain DAT by [^{11}C]PE2I and PET in human and nonhuman primates [11, 12]. Changes in DAT binding in Parkinson's disease, attention-deficit/hyperactivity disorder (ADHD) and schizophrenia have also been observed using [^{123}I]PE2I [13, 14] and [^{11}C]PE2I [15–17], respectively. Quantitative analysis using both arterial input function and reference tissue in humans has been reported with [^{123}I]PE2I [18, 19] and [^{11}C]PE2I [20–22]. It has been reported that the binding potential (BP_{ND}) values of striatal regions are underestimated by the simplified reference tissue model (SRTM) method [20, 23] compared with those by kinetic analysis and Logan analysis with use of arterial input function in [^{11}C]PE2I PET studies [20–22]. However, neither the cause of the underestimation with SRTM nor the applicability of SRTM to other brain regions has as yet been investigated in detail.

In this study, we attempted to validate quantification methods using a reference tissue model in [^{11}C]PE2I PET studies with both measured PET data and simulated data. In addition to SRTM, the original multilinear reference tissue model (MRTMo) [24] was applied to estimate the distribution volume ratio (DVR), instead of BP_{ND}, and compared by quantitative analysis using arterial input function.

Materials and methods

Calculation of specific binding

Specific binding of [^{11}C]PE2I to DAT can be evaluated by the tracer DVR of the target brain region to the reference tissue region showing negligible specific binding according to the following equation:

$$DVR = \frac{V_T}{V_T'} \tag{1}$$

where V_T and V_T' are the distribution volumes of the target brain and reference region, respectively. The distribution volume can be estimated using kinetic analysis and plasma-input Logan analysis with arterial input function.

Quantification using arterial input function

Kinetic analysis

To describe the [^{11}C]PE2I kinetics in the brain regions, the 2-tissue model consisting of plasma and two tissue components (2-tissue model) was used [22, 25–27]. In this model, the following equations are expressed:

$$C_T(t) = C_{ND}(t) + C_S(t), \tag{2}$$

$$\frac{dC_{ND}(t)}{dt} = K_1 C_p(t) - k_2 C_{ND}(t) - k_3 C_{ND}(t) + k_4 C_S(t), \tag{3}$$

$$\frac{dC_S(t)}{dt} = k_3 C_{ND}(t) - k_4 C_S(t). \tag{4}$$

C_T is the total radioactivity concentration in the brain tissue, C_{ND} is the radioactivity concentration of nondisplaceable radioligand in the brain tissue, which includes nonspecifically bound and free radioligand concentrations, C_S is the radioactivity concentration of the radioligand specifically bound to DAT, and C_p is the radioactivity concentration of the unchanged radioligand in plasma (arterial input function). The rate constants K_1 and k_2 describe the influx and efflux rates for radioligand diffusion through the blood–brain barrier (BBB), respectively. The rate constants k_3 and k_4 represent the radioligand transfer between the compartments for nondisplaceable radioligand and specific radioligand binding to receptors, respectively.

For the 1-tissue model, K_1 and k_2 are the influx and efflux rates for radioligand diffusion through BBB:

$$C_T(t) = C_{ND}(t), \tag{5}$$

$$\frac{dC_{ND}(t)}{dt} = K_1 C_p(t) - k_2 C_{ND}(t). \tag{6}$$

Total distribution volume (V_T) denotes the tracer concentration ratio of tissue to plasma under equilibrium condition. V_T is calculated for the 2-tissue model as follows:

$$V_T = \frac{K_1}{k_2}\left(1 + \frac{k_3}{k_4}\right). \tag{7}$$

For the 1-tissue model:

$$V_T = \frac{K_1}{k_2}. \tag{8}$$

Additionally, V_b (ml/ml) was introduced as the fractional volume of blood space in the region. Then measured radioactivity concentration of the region with PET is expressed as,

$$C_{ROI}(t) = V_b C_b(t) + (1 - V_b)C_T(t) \tag{9}$$

where $C_{ROI}(t)$ and $C_b(t)$ are the measured radioactivity concentrations of the region and total blood, respectively. Each kinetic parameter, including V_b, was estimated by nonlinear least-squares fitting procedure without weighing. For the cerebellum, the 1-tissue model was also applied. The appropriate model of the cerebellum was evaluated by the Akaike information criterion [28].

Plasma-input Logan analysis

The total distribution volume was calculated by plasma-input Logan analysis developed by Logan et al. [29]. After an equilibrium time (t^*), the following linear relationship is obtained:

$$\frac{\int_0^t C_T(s)ds}{C_T(t)} = a \frac{\int_0^t C_p(s)ds}{C_T(t)} + b \quad (t > t^*), \qquad (10)$$

where the slope a denotes the total distribution volume. In this analysis, t^* was determined so that the maximum discrepancy from the regression line within the linear segment would be 10% for each time–activity curve (TAC). To test the possible underestimation of striatal V_T generated by too early t^*, the caudate TAC of the earliest t^* was re-estimated with fixed t^* at the latest one.

Quantification using reference tissue data without arterial input function

To avoid measurements of arterial input function, noninvasive analysis employing a reference region with negligible specific binding was applied. *DVR* is derived from the TACs of the brain regions and reference region. In the case of DAT, the cerebellum was reported not to express any mRNA [30]. Pretreatment and blocking studies of [11C]PE2I in monkeys showed no changes in cerebellar TACs [11]. Therefore, the cerebellum was used as a reference brain region. In this study, MRTMo and SRTM were applied to calculate *DVR*.

MRTMo method

MRTMo is one of the variations of the graphical approach. After a certain equilibrium time (t^*), the following multilinear regression is obtained:

$$\frac{\int_0^t C_t(s)ds}{C_t(t)} = \frac{a}{a'} \frac{\int_0^t C_{ref}(s)ds}{C_t(t)} + \left(-\frac{ab'}{a'}\right)\frac{C_{ref}(t)}{C_t(t)} + b, \qquad (11)$$

where C_t and C_{ref} are tissue radioactive concentrations of the target brain and reference regions, respectively, a and a' are the distribution volumes of the target brain and the reference regions, respectively, and therefore a/a' denotes *DVR*. b' and b are $-1/k_2'$ and $-1/k_2$, respectively, where k_2'

is k_2 of the reference region. The time t^* was determined in the same way as described in the plasma-input Logan analysis previously.

SRTM method

In the SRTM method, *DVR* can be determined by modification of the original SRTM equation as follows:

$$C_t(t) = R_1 C_{ref}(t) + \left(R_1 k_2' - R_1 \frac{R_1 k_2'}{DVR}\right) C_{ref}(t)$$
$$\otimes \exp\left(-\frac{R_1 k_2'}{DVR}t\right), \qquad (12)$$

where R_1 is K_1/K_1' and K_1' is K_1 of the reference tissue. *DVR* is calculated by the non-linear least-squares fitting procedure.

All of the analysis described above was performed with PMOD Ver. 2.6 (PMOD Technologies, Zürich, Switzerland).

Preparation of [11C]PE2I

[11C]PE2I was synthesized by *O*-methylation of the corresponding precursors with [11C] methyl iodide with ultra-high specific activity, which was obtained by a reduction of [11C]CO$_2$ with LiAlH$_4$ in an inert atmosphere with specially designed equipment [31], and automatically purified [32].

Subjects

Six healthy male volunteers (age 20–28 years, 23.8 ± 3.1, mean ± SD) participated in this study. All subjects underwent 1.5 T T1-weighted MRI examinations to obtain anatomical brain references for the PET images. The MRI scanner was Intella (Philips Medical Systems, Best, The Netherlands). Three-dimensional volumetric acquisition of a T1-weighted gradient echo sequence produced a gapless series of thin transverse sections (TE: 9.2 ms; TR: 21 ms; flip angle: 30°; field of view: 256 mm, acquisition matrix: 256 × 256; slice thickness: 1 mm). None of the subjects had a significant medical history or brain morphological abnormalities. This study was performed in compliance with the Declaration of Helsinki and approved by the Ethics and Radiation Safety Committees of the National Institute of Radiological Sciences, Chiba, Japan. Written informed consent was obtained from all subjects prior to the study.

PET measurement

PET data were acquired using an ECAT EXACT HR+ (CTI-Siemens, Knoxville, TN, USA) in 3-dimensional

mode, which provides 63 sections with an axial field of view of 15.5 cm [33]. The intrinsic in-plane and axial resolutions were 4.3 and 4.2 mm full width at half maximum (FWHM), respectively. The dynamic PET image data were corrected for physical decay of ^{11}C. An individualized thermal plaster mouthpiece and nose plate were used for head immobilization during the PET scanning. A cannula was inserted into the brachial artery for arterial blood sampling. Prior to the emission scan, a 10-min transmission scan was performed using a ^{68}Ge–^{68}Ga rod source. After intravenous rapid bolus injection of [^{11}C]PE2I, a 90-min dynamic PET scan was performed (35 frames: 9×20 s, 5×1 min, 4×2 min, 12×4 min, 5×6 min). The injected dose and specific radioactivity were 197–230 MBq and 644–1104 GBq/μmol at the time of injection, respectively. The emission data were reconstructed with a Hanning filter (cutoff frequency: 0.4 cycle/pixel), and the reconstructed in-plane resolution was 7.5 mm FWHM.

Arterial input function

Frequent arterial blood sampling was performed throughout the scan. For the first 5 min after the injection, arterial blood was withdrawn using a peristaltic pump at a constant rate to monitor whole blood radioactivity with an automatic radioactive monitoring system [34] simultaneously with blood sampling at the end of the tube. The sampling time points after the tracer injection were as follows: every 10 s from 15 to 105 s, then 120, 150, 180 s and every 1 min from 4 to 6 min, every 2 min from 6 to 12 min, 15, 20 min and every 10 min from 20 to 90 min. The radioactivity in each sample was measured with a well-type auto-gamma counter (COBRA II Auto Gamma, Packard Instrument Co., Meriden, CT, USA) to obtain the radioactive concentration in whole blood. Then the blood samples were centrifuged, and an aliquot of plasma was taken to measure the total radioactive concentration in plasma. The sensitivities of the continuous monitoring system and well-type gamma counter were cross-calibrated with that of the PET system.

Radioactive fractions of unmetabolized [^{11}C]PE2I in plasma were evaluated by HPLC radiochromatography. Arterial blood samples taken at 3.5 min and every 10 min from 9 to 89 min after the tracer injection were centrifuged and a 1-mL aliquot of plasma was added with the same amount of acetonitrile. The mixture was vortexed and centrifuged at 13000 rpm for 2 min with a refrigerated centrifuge. Then an aliquot of 0.5 mL of the supernatant was injected into the HPLC system (GL Sciences Inc., Tokyo, Japan). The analytical column was Waters μBondapak C18 (300×7.5 mm i.d.), the mobile phase was acetonitrile and 0.1 M ammonium formate (70/30) at an isocratic condition, and the flow rate was 6.0 mL/min. The radiochromatography peak of [^{11}C]PE2I was identified

by standard PE2I at the detection wavelength of 254 nm. The unchanged fraction was calculated as the peak area ratio of unchanged [^{11}C]PE2I to the total peaks detected. The time course of unchanged [^{11}C]PE2I fraction was approximated by a power function ($y(t) = At^{-b}$; $y(t) = 1$ when $At^{-b} > 1$ during the first few minutes) individually. The arterial input function was obtained as the product of plasma radioactive concentration and the unchanged fraction. The time lag between brain TACs and input function was adjusted at their onsets individually. Plasma protein binding was not determined in the present study.

Regions of interest

T1-weighted MRI images were coregistered and resliced to PET images using SPM2 [35]. Polygonal regions of interest (ROIs) were drawn on the MRI images and placed on the PET summation images. The regions chosen in this study were the cerebellum, pons, temporal cortex, frontal cortex, occipital cortex, parietal cortex, caudate head, thalamus, putamen, midbrain, parahippocampal gyrus, anterior part of the cingulate gyrus, and white matter (central semiovale). Then the ROIs were placed on the dynamic PET images to obtain regional TACs. The TACs were corrected for physical decay of ^{11}C.

Simulation study

To estimate errors in *DVR* calculated by the reference tissue models for [^{11}C]PE2I kinetics in human brain, a simulation study was performed. Brain TACs were generated using assumed kinetic parameters taken from the results of the kinetic analysis of [^{11}C]PE2I. For the reference region, kinetic parameters were assumed for both 1- and 2-tissue models. Kinetic parameters of the reference region were set as $K_1' = 0.25$, $K_1'/k_2' = 2$, $k_3' = 0.0089$ and $k_4' = 0.019$ for the 2-tissue model, and $K_1' = 0.25$ and $K_1'/k_2' = 2$ for the 1-tissue model. The simulation results when the reference tissue kinetics as the 1-tissue model at $K_1'/k_2' = 2.45$ was similar to those of $K_1'/k_2' = 2.0$ (data not shown). To highlight the contribution of the second tissue compartment of the reference region, a uniform K_1'/k_2' value was applied. Also, despite the fact that the K_1/k_2 values of striatal regions were approximately fivefold higher than those of other regions, K_1/k_2 and k_4 of the target brain region parameters were assumed to be the same values as the reference region parameters. The result of the preliminary simulation using $K_1/k_2 = 10$ was similar to that of $K_1/k_2 = 2.0$ (data not shown). K_1 of the target region was fixed at 0.20 and k_3 was varied to alter *DVR*. The range of k_3 was from 0.0005 to 0.35 in 26 steps or 0.01–0.55 in 24 steps when the reference tissue kinetics was for the 1-tissue or 2-tissue model, respectively, to

cover the *DVR* range from 1.03 to 20. The fractional blood volume (V_b) was fixed at 0.04 mL/mL for all conditions. A typical metabolite-corrected input function and whole blood TAC were used to generate TACs. The assumed *DVR* was determined as the ratio of V_T calculated by Eq. 7 of the target brain region to that of the reference region. For each simulated TAC, *DVR* was estimated by MRTMo and SRTM and compared to the corresponding assumed *DVR* value. Another simulation was performed to test whether the scan duration of 90 min was sufficient when the reference region kinetics was according to the 2-tissue model.
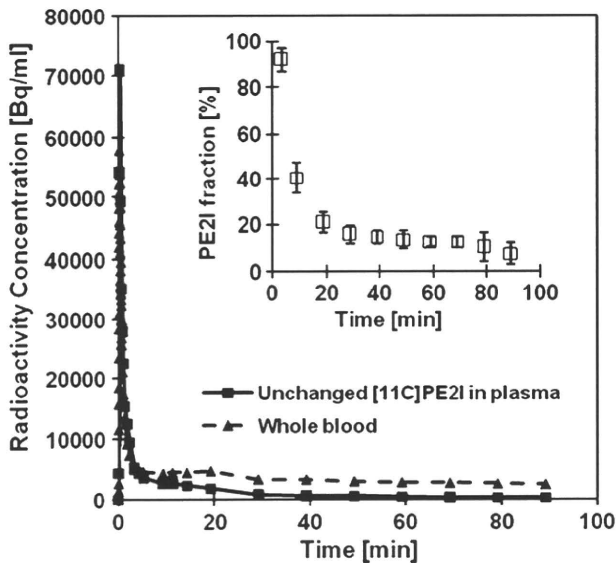
The input function was exponentially extrapolated with a single exponential to 240 min (4 h) using 30–90-min data, and 4-h target tissue curves were generated in the same manner as described above. Then, *DVR* was estimated by MRTMo and SRTM. For MRTMo, in addition to the determination of t^* as the time when the percentage deviation from the model was within 10% for each case, *DVR* was calculated when t^* was fixed at 120 min for all cases.
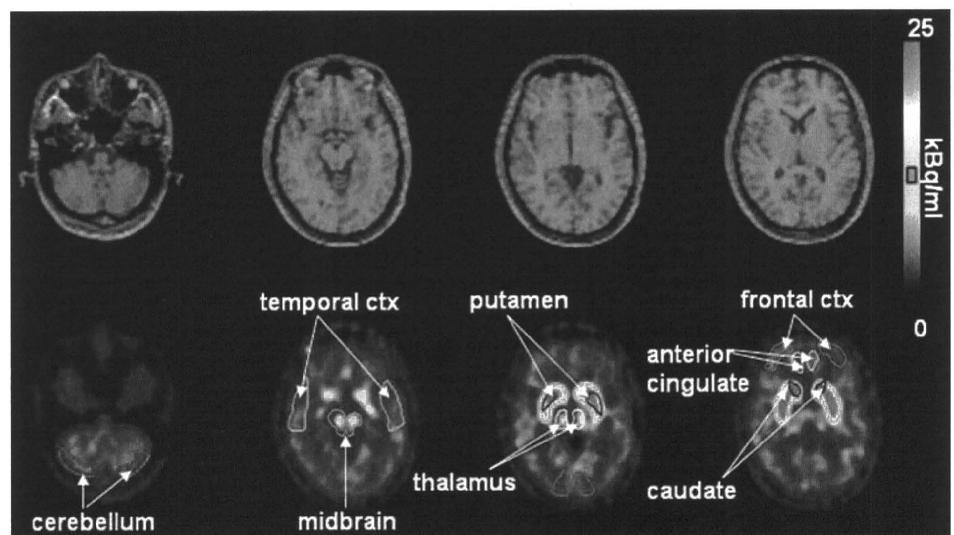
Results

Input function

Figure 1 shows the typical time course of the radioactive concentration of whole blood and that of unchanged [^{11}C]PE2I in plasma. The average time course of the unchanged fraction is also shown. The metabolism of [^{11}C]PE2I is relatively fast, and so the unchanged [^{11}C]PE2I fraction was 25% at 20 min after injection and continued to decline gradually until the end of the scan.

PET images and ROIs

A typical example of PET images of [^{11}C]PE2I obtained by summation of the frames from 0 to 90 min after injection and coregistered T1-weighted MRI images is shown in Fig. 2. Higher radioactivity concentrations were observed in the caudate head and putamen, regions known to be rich in DAT. Among other regions, the midbrain and thalamus showed some [^{11}C]PE2I binding, whereas the cerebellum and other cortical regions demonstrated very little.

Fig. 1 Arterial input function. Typical time–activity curves of arterial whole blood (*filled triangles*) and unchanged [^{11}C]PE2I in plasma (*filled circles*). The *inset* is the mean fraction of unchanged [^{11}C]PE2I in plasma obtained from the 6 subjects. The *error bars* indicate 1 standard deviation

Fig. 2 Coregistered T1-weighted MRI images and [^{11}C]PE2I images (summed image of 0–90 min) with ROIs

Brain TACs

Typical TACs of various cerebral regions are shown in Fig. 3. Marked [^{11}C]PE2I uptake and retention are observed in the putamen. Midbrain and thalamus showed slower clearance than the cerebellum and other cortical regions, and radioactivity concentrations in the midbrain and thalamus were higher than in other regions at the end of the scan, with the lowest observed in the cerebellum. The TAC of the putamen reached a plateau within 90 min after the injection in all subjects, indicating the reversibility
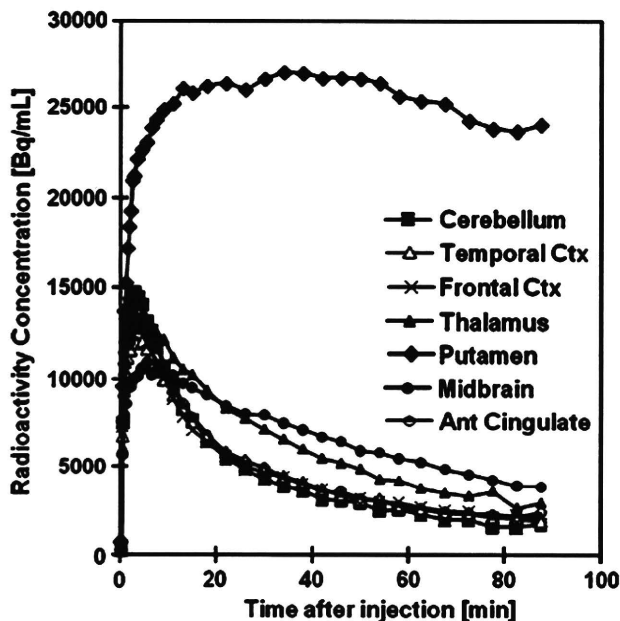

Fig. 3 Typical time–activity curves of [^{11}C]PE2I in the human brain

of this tracer. In other regions, TACs attained peaks a few minutes after the injection and then declined faster than that of the putamen.

Kinetic analysis and plasma-input Logan analysis

TACs of all ROIs were well described by the 2-tissue model. Table 1 shows the mean kinetic parameters obtained by kinetic analysis with 2-tissue model analysis. For the cerebellum, kinetic analysis with the 1-tissue model was also applied. Figure 4 shows a cerebellar TAC and the fitted curves with 1- and 2-tissue models, respectively. The mean kinetic parameters of the 1-tissue model were $V_b = 0.0544$ ml/ml, $K_1 = 0.252$ ml/min/ml, $k_2 = 0.104$/min and $V_T = 2.45$ ml/ml. The mean AICs of the 1-tissue and 2-tissue models were 563 and 519, respectively. Since the mean AIC of the 2-tissue model was significantly lower than that of the 1-tissue model by paired t test ($P < 0.0005$), the 2-tissue model was preferred over the 1-tissue model for describing the cerebellar TAC. The mean K_1/k_2 values of striatal regions were 9.79 (caudate) and 11.2 (putamen), and were significantly higher than those of other regions (approximately 2.0). In addition, the coefficients of variation of K_1/k_2 in striatal regions were 47.9% (caudate) and 23.5% (putamen), whereas those of other regions ranged from 10.6 to 16.8%, except for pons (26.6%) and white matter (26.5%).

Plasma-input Logan analysis was also performed to obtain the distribution volume (V_T). Typical examples of plasma-Logan plot for putamen and midbrain are shown in Fig. 5. V_T values obtained by kinetic analysis and plasma-input Logan analysis are shown in Table 1. The t^* of striatal regions ranged from 24 to 52 min. The caudate

Table 1 Mean kinetic parameters and total distribution volumes estimated by each analysis in humans ($n = 6$)

Region	2-Tissue model analysis						Graphical analysis
	V_b (ml/ml)	K_1 (ml/min/ml)	k_2 (/min)	k_3 (/min)	k_4 (/min)	V_T (ml/ml)	V_T (ml/ml)
Cerebellum	0.0318 (14.7)	0.264 (18.7)	0.128 (21.3)	0.00892 (59.0)	0.0189 (54.1)	3.08 (15.7)	2.79 (18.1)
Pons	0.0325 (28.9)	0.217 (17.8)	0.107 (39.8)	0.0213 (67.9)	0.0286 (74.3)	4.45 (46.6)	3.38 (21.9)
Temporal cortex	0.0405 (17.4)	0.211 (15.4)	0.109 (22.7)	0.0115 (55.8)	0.0151 (75.4)	4.43 (49.4)	2.96 (10.5)
Frontal cortex	0.0371 (18.0)	0.236 (16.7)	0.130 (24.0)	0.0152 (45.3)	0.0168 (36.2)	3.50 (16.7)	3.12 (17.6)
Occipital cortex	0.0239 (53.5)	0.244 (12.2)	0.126 (23.8)	0.0125 (32.0)	0.0159 (30.9)	3.59 (18.8)	3.18 (17.0)
Caudate	0.0346 (19.5)	0.252 (19.5)	0.0336 (60.6)	0.0936 (122)	0.0178 (34.7)	43.2 (25.9)	35.3 (22.9)
Thalamus	0.0299 (41.1)	0.262 (25.6)	0.153 (83.3)	0.0781 (202)	0.0409 (85.9)	3.77 (18.0)	3.49 (20.9)
Putamen	0.0394 (24.7)	0.276 (23.1)	0.0269 (47.2)	0.0441 (54.7)	0.0143 (24.6)	42.9 (21.7)	33.7 (30.8)
Midbrain	0.0366 (25.1)	0.161 (18.0)	0.0810 (36.4)	0.0441 (71.0)	0.0347 (34.3)	4.54 (20.7)	4.23 (17.9)
Parahippocampal gyrus	0.0422 (14.8)	0.160 (21.3)	0.0859 (27.9)	0.0126 (64.1)	0.0196 (65.5)	2.98 (22.9)	2.78 (22.7)
Anterior cingulate	0.0434 (16.9)	0.234 (20.6)	0.118 (20.7)	0.0137 (38.2)	0.0165 (35.8)	3.65 (14.6)	3.12 (17.4)
Parietal cortex	0.0396 (14.0)	0.248 (16.7)	0.128 (22.2)	0.0119 (38.6)	0.0140 (37.2)	3.68 (15.2)	3.15 (14.1)
White matter	0.0136 (15.9)	0.093 (24.5)	0.0821 (43.9)	0.0756 (79.4)	0.0319 (15.7)	3.78 (16.5)	3.62 (20.1)

Mean and coefficient of variation in *parentheses* are expressed as mean value and normalized SD of each parameter for six subjects
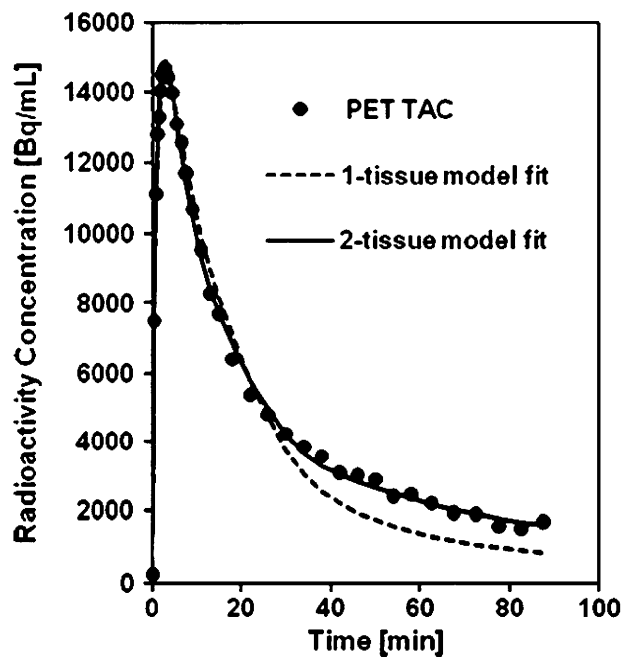
Fig. 4 Typical example of cerebellar time–activity curve and fitted model curves. *Filled circles, solid line* and *dashed line* represent measured time–activity curves, the 2-tissue model curve and the 1-tissue model curve, respectively. The estimated parameters for 1-tissue model fit were $V_b = 0.0521$ ml/ml, $K_1 = 0.302$ ml/min/ml and $k_2 = 0.132$/min. Those for 2-tissue model fit were $V_b = 0.0269$ ml/ml, $K_1 = 0.320$ ml/min/ml, $k_2 = 0.161$/min, $k_3 = 0.00824$/min and $k_4 = 0.0167$/min. The resultant AIC for 1-tissue model fit and 2-tissue model fit were 585 and 532, respectively

TAC of $t^* = 24$ min was re-analyzed with fixed t^* at 52 min. The estimated V_T values were 34.2 ml/ml ($t^* = 24$ min) and 35.7 ml/ml ($t^* = 52$ min), respectively. The relative difference generated by longer t^* was about 4%. t^* of other regions ranged from 7 min (thalamus) to 32 min (occipital). Overall, V_T values obtained by plasma-input Logan analysis were lower than those by kinetic analysis (approximately, 20% underestimation).

Reference tissue model analysis (noninvasive analysis)

With the SRTM method, 5 of 60 brain TACs, except the caudate and putamen, failed to converge and were excluded from further evaluation. The relationship between *DVR* obtained by plasma-input Logan analysis and the reference tissue models is presented in Fig. 6a. The estimated *DVR* was found to be underestimated in the striatal regions showing high *DVR*. Figure 6b focused on the lower *DVR* part of Fig. 6a. In the lower *DVR* range, *DVR* values were consistent between plasma-input Logan analysis and the reference tissue model methods ($R^2 = 0.940$ for MRTMo and $R^2 = 0.607$ for SRTM, respectively). The regional *DVR*s estimated with MRTMo and SRTM in low *DVR* regions are summarized in Table 2. The time t^* of MRTMo
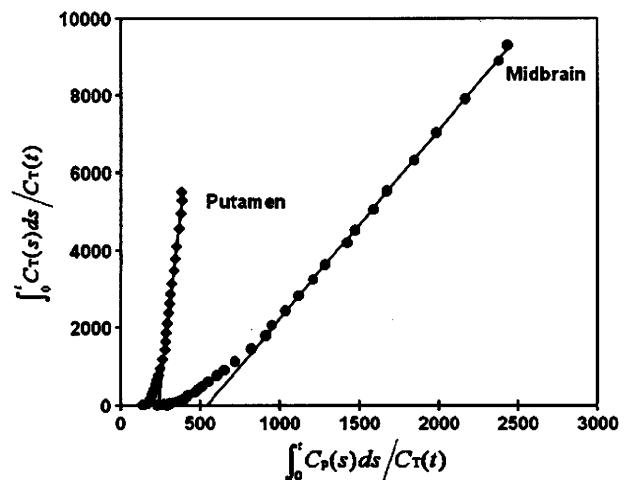

Fig. 5 Examples of plasma-Logan plot of the TACs in Fig. 3. For the putamen, t^* was 52 min, and V_T estimated with plasma-Logan analysis was 34.3 ml/ml, whereas V_T estimated with the 2-tissue compartment model was 40.8 ml/ml. For the midbrain, t^* was 24 min and V_T estimated with plasma-Logan analysis was 5.11 ml/ml, whereas V_T estimated with the 2-tissue compartment model was 4.84 ml/ml

ranged from 3.5 min (thalamus) to 26 min (pons and anterior cingulate).

Simulation study

The relationship between the estimated *DVR* by MRTMo and SRTM methods and assumed *DVR* calculated with kinetic parameters, with tracer kinetics in the reference region being described by the 2-tissue model, is shown in Fig. 7a and b. The relationship was curvilinear, similar to the result of the clinical study. Consequently, when assumed *DVR*s were 9.64 and 20.4, estimated *DVR*s were 6.91 (28.3% underestimation) and 11.2 (45.1% underestimation) by MRTMo, and 7.26 (24.7% underestimation) and 11.1 (45.6% underestimation) by SRTM, respectively. Though there was underestimation in the high *DVR* range, Fig. 7b also demonstrated the applicability of the reference tissue models in a lower *DVR* range. The time t^* of MRTMo ranged from 1.5 min to 18 min. t^* of *DVR*s over 10, corresponding to those of striatal regions, ranged from 5.5 to 13 min and were comparable to the human results. When tracer kinetics in the reference region was described by the 1-tissue model, the relationship between estimated and assumed *DVR* became almost linear for the entire *DVR* range (Fig. 7c).

The results of the simulation for the extended scan duration up to 4 h, when the reference tissue kinetics was the 2-tissue model, are shown in Fig. 7d. When the assumed *DVR*s were 9.64 and 20.4, estimated *DVR*s were 7.89 (18.1% underestimation) and 14.0 (31.4%

Fig. 6 a The relationship between *DVR* obtained by plasma-input Logan analysis and the reference tissue models. Low *DVR* range is zoomed up in (b). The *solid line* is the regression line for MRTMo
($y = 0.901x + 0.077$, $R^2 = 0.940$) and the *dashed line* is that for SRTM
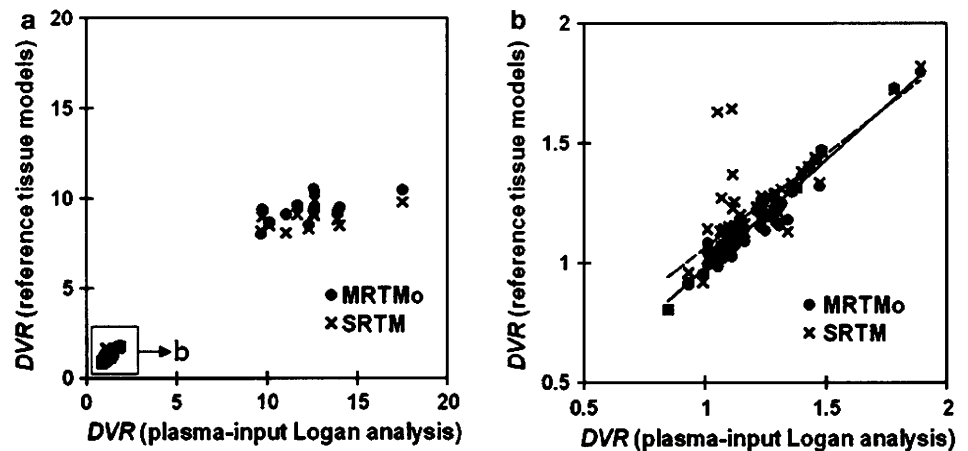($y = 0.785x + 0.275$, $R^2 = 0.607$)

Table 2 Distribution volume ratios obtained by graphical analysis and reference tissue models

REGION	Graphical analysis		MRTMo		SRTM	
	Mean	SD	Mean	SD	Mean	SD
Pons	1.21	0.14	1.19	0.12	1.16	0.12
Temporal cortex	1.08	0.10	1.03	0.07	1.03	0.07
Frontal cortex	1.12	0.06	1.07	0.04	1.26	0.21
Occipital cortex	1.15	0.12	1.09	0.08	1.20	0.08
Thalamus	1.25	0.13	1.27	0.11	1.25	0.11
Midbrain	1.53	0.25	1.48	0.23	1.37	0.22
Parahippocampal gyrus	0.996	0.100	0.971	0.104	1.03	0.04
Anterior cingulate	1.12	0.10	1.11	0.07	1.15	0.08
Parietal cortex	1.14	0.09	1.08	0.06	1.22	0.29
White matter	1.30	0.13	1.22	0.08	1.20	0.07

underestimation) by SRTM, and 8.65 (10.3% underestimation) and 17.5 (14.2% underestimation) by MRTMo with t^* determined within 10% discrepancy, respectively. The time t^* ranged from 1.5 to 42 min. For both reference tissue models, longer scan duration reduced the underestimation of the *DVRs*. Then, MRTMo with fixed t^* at 120 min was applied, and the estimates for assumed *DVRs* of 9.64 and 20.4 were 8.99 (6.74% underestimation) and 18.7 (8.33% underestimation), respectively. On comparing Fig. 7d with Fig. 7a, the curves became more linear and the underestimation was recovered with longer scan duration, and especially the *DVR* estimated with MRTMo with fixed t^* at 120 min. Therefore, MRTMo with delayed t^* improved the underestimation significantly.

Discussion

Regional distribution of [^{11}C]PE2I in brain was in good agreement with the known distribution of DAT in post-mortem brain [36], supporting the contention that [^{11}C]PE2I-PET imaging is an appropriate technique for visualizing DAT distribution in human brain in vivo. The ratio of radioactive concentration in the putamen to that in the cerebellum was approximately 10 at the end of the scan. These results were in agreement with a previous human PET study [22]. Estimated V_T values of striatal regions and midbrain were lower than those in previous reports [21, 22]. On the other hand, V_T of the cerebellar cortex was similar. The V_T values of the highly accumulated, small regions depend on the ROI determined and the special resolution of the PET scanner. Though the ROI delineations of the two reports were not shown, differences in the ROI delineations can be one of the reasons for such discrepancies. Another possible explanation is that since Hirvonen et al. used a high-resolution PET scanner, the partial volume effect, which causes the underestimation of V_T, may have been less marked.

Quantification using arterial input function

Although it is generally assumed that the tracer kinetics in the reference region is based on the 1-tissue model, the 2-tissue model was considered superior for describing the TAC in the cerebellum as reported previously [20, 22]. Recently, two radioactive metabolites of [^{11}C]PE2I were identified in rat brain tissue 30 min after intravenous administration of [^{11}C]PE2I [37]. One was reported to be pharmacologically active hydroxylated PE2I ([^{11}C]1) and the other inactive carboxyl-desmethyl-PE2I ([^{11}C]2). The report showed that [^{11}C]PE2I was stable in rat brain homogenates and that liver cytochrome P450 enzymes were responsible for the formation of [^{11}C]1, and also that [^{11}C]2 was a metabolite of [^{11}C]1 through alcohol and aldehyde dehydrogenases. [^{11}C]1 is considered to enter the brain across BBB from plasma in rats, and more polar [^{11}C]2 is considered to be transformed within the brain from [^{11}C]1. Nevertheless, although the metabolism and

Fig. 7 a Simulation results of the relationship between theoretical *DVR* and estimated *DVR* by the reference tissue models when reference tissue kinetics is the 2-tissue model. **b** Zoom-up of lower *DVR* range of **a**. The *solid* and *dashed lines* are regression lines for MRTMo ($y = 0.802x + 0.268$) and SRTM ($y = 0.880x + 0.141$). **c** Simulation results of the relationship between theoretical *DVR* and estimated *DVR* by the reference tissue models when reference tissue kinetics is the 1-tissue model. **d** Simulation results of the relationship between theoretical *DVR* and estimated *DVR* when extended scan duration of 4 h was applied and the reference tissue kinetics is the 2-tissue model. The *solid line* and *dashed line* are regression lines for MRTMo with fixed t^* at 120 min ($y = 0.914x + 0.128$)
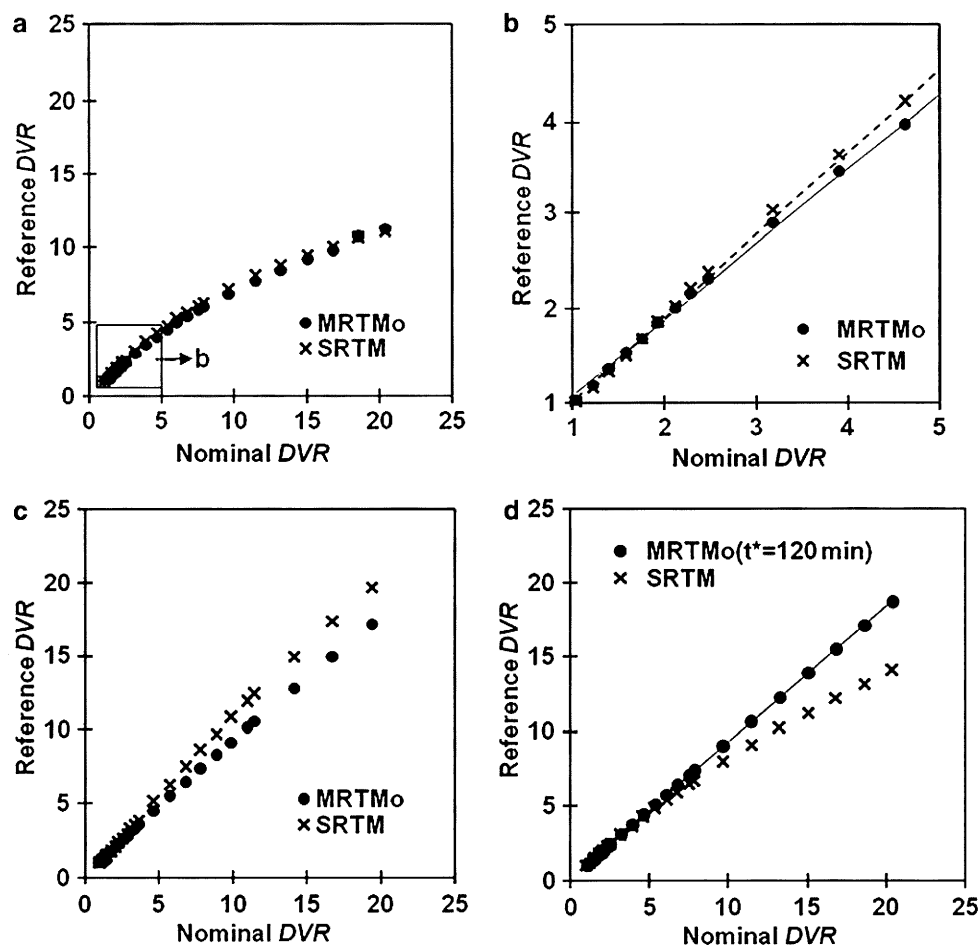
pharmacokinetics of [^{11}C]PE2I and BBB-permeability in humans may be considered different from those in rats, this cannot directly indicate that a BBB-permeable metabolite accumulated in the human brain and affected the kinetics. For the discrepancy of K_1/k_2 values between striatal regions and the other regions, the larger coefficients of variation implied that the curve fitting of these high V_T regions was somewhat unstable. On the other hand, the curve fitting using the constrained K_1/k_2 values of the cerebellum even worsened the goodness of fit for all cases (data not shown). Therefore, K_1/k_2 values of striatal regions are unlikely to be the same as that of the cerebellum.

Though various t^* values were determined across the regions in plasma-input Logan analysis, V_T values were insensitive to t^*. Therefore, uniform t^*, for example 30 min, can be applied to all regions. The estimated distribution volumes by kinetic analysis and plasma-input Logan analysis were in good agreement, although the values by the latter were systematically lower than those by the former. It was considered that 90 min was an insufficient scan time for the estimation of V_T with plasma-input Logan analysis as described in a recent study [20], in addition to the noise-induced underestimation [38]. In

some cases in kinetic analysis, extremely small k_4 values (<0.01, approximately half of the averaged k_4) generated significantly large V_T values in kinetic analysis. Consequently, large discrepancies of estimated V_T values between kinetic analysis and plasma-input Logan analysis and relatively larger coefficients of variation for V_T derived by kinetic analysis than those by plasma-input Logan analysis occurred. Therefore, V_T estimated by plasma-input Logan analysis was considered more suitable to validate *DVR* estimation with the reference tissue models.

Reference tissue model methods

Underestimation of *DVR* was observed in regions with high *DVR*, i.e., the striatum for both reference tissue model methods MRTMo and SRTM as compared with plasma-input Logan analysis and kinetic analysis in the measured data as shown in Fig. 6a. Previous reports also showed underestimation of BP_{ND} in the striatum obtained with SRTM [20–22]. One of the reasons for this underestimation was considered to be the fact that the tracer kinetics in the cerebellum could be described by the 2-tissue model, while the assumption of both of the reference tissue models was

that the kinetics of the reference tissue must be described with the 1-tissue model. The results of the simulation study shown in Fig. 7a and c indicates that the TAC of the reference region underlies the underestimation of high DVR. Such underestimation of BP_{ND}, which is equivalent to DVR-1, calculated by SRTM was also reported in PET studies with [carbonyl-^{11}C]WAY-100635, a 5-HT$_{1A}$ receptor ligand [39].

On the other hand, in the regions with low DVR, both the human and 90-min simulation studies showed that DVR estimated with the reference tissue models was well correlated with those calculated with plasma-input Logan analysis despite the violation of the assumption of the reference tissue model methods (Figs. 6b, 7b). Therefore, these methods were thought to be practically applicable under certain conditions, though the reference tissue TAC was well fitted by the 2-tissue model. Since [^{11}C]PE2I kinetics in the striatal regions is slow, we speculated that the underestimation of high DVR could be remedied by a longer PET data duration if physical decay of the radioisotope was allowed. The simulation extending scan duration up to 4 h showed that the underestimation could be improved by longer scan time for both methods; especially, DVRs estimated with MRTMo applying prolonged t^* were linearly correlated with assumed DVRs with a slope of 0.91 (Fig. 7d). The further improvement of the underestimation by MRTMo with prolonged t^* implies that the contribution of the latter part of the TACs was involved in the estimation of closer DVR to that of analysis using plasma-input function. Therefore, it is suggested that higher DVR estimation with the reference tissue models requires an even longer acquisition time than does the analysis using plasma-input function when reference tissue TAC is described with a 2-tissue model. However, in practice, the physical decay of ^{11}C limits the scan duration to up to 90 min.

For SRTM, it was possible to raise underestimated DVR by constraining lower k'_2 for 90-min data. For some other established reference tissue model methods, which need predetermined k'_2, DVR can be raised by giving smaller k'_2. Such application may remedy the underestimation of high DVR for 90-min data, but the validation must be carefully done.

For the estimation of lower DVR with the reference tissue models, 90-min scan was considered a sufficient duration. Ichise et al. [40] investigated the bias and variability of BP_{ND} estimated with several reference tissue models by simulations. They showed that MRTMo produced a variability of 5%, negative bias of 11.4% and no outliers (e.g., nonconvergent case) for a TAC with 5% noise, whereas SRTM produced 35.6% variability, 6.7% positive bias and some outliers at the same noise level when $BP_{ND} = 0.27$ ($DVR = 1.27$). In the present study, though no extreme outliner was generated, there were some nonconvergent data in the SRTM estimation results. This

suggests that MRTMo reveals more stable BP_{ND} (DVR) but produces noise-dependent underestimation, and also that SRTM is somewhat unstable but has less deviation when BP_{ND} (DVR) is low. Yet, the simulation study indicated that SRTM estimates were in closer agreement with the nominal values than MRTMo estimates (Fig. 7b).

The previous study of Hirvonen et al. [21] reported excellent reproducibility in BP_{ND} of thalamus and midbrain estimated with SRTM. In the present study, both the measured and simulated data demonstrated consistency between the reference tissue models and plasma-input Logan analysis using arterial input function for 90-min data duration. Taken together, with some cautions as described above, the noninvasive approaches appear to be applicable and feasible for evaluating specific binding of [^{11}C]PE2I in lower binding regions including the midbrain and thalamus.

Conclusion

The use of SRTM and MRTMo for the estimation of DVRs of low-binding regions is a feasible noninvasive analysis for 90-min scan time for [^{11}C]PE2I despite the violation of the assumption of the reference tissue models. The simulation study suggested that the estimation of high DVR such as of striatal regions, the [^{11}C]PE2I kinetics of which is slower, needed further data duration, which is an unrealistic situation for the ^{11}C-labeled ligand. Taken together, [^{11}C]PE2I is a useful radioligand to evaluate DAT activity in lower binding regions such as the midbrain and thalamus.

References

1. Fowler JS, Volkow ND, Wolf AP, Dewey SL, Schlyer DJ, Macgregor RR, et al. Mapping cocaine binding sites in human and baboon brain in vivo. Synapse. 1989;4(4):371–7.
2. Hantraye P, Brownell AL, Elmaleh D, Spealman RD, Wullner U, Brownell GL, et al. Dopamine fiber detection by [^{11}C]-CFT and PET in a primate model of Parkinsonism. Neuroreport. 1992;3(3):265–8.
3. Wong DF, Yung B, Dannals RF, Shaya EK, Ravert HT, Chen CA, et al. In vivo imaging of baboon and human dopamine transporters by positron emission tomography using [11C]WIN 35, 428. Synapse. 1993;15(2):130–42.

4. Muller L, Halldin C, Farde L, Karlsson P, Hall H, Swahn CG, et al. [^{11}C] beta-CIT, a cocaine analogue. Preparation, autoradiography and preliminary PET investigations. Nucl Med Biol. 1993;20(3):249–55.

5. Halldin C, Farde L, Lundkvist C, Ginovart N, Nakashima Y, Karlsson P, et al. [^{11}C]beta-CIT-FE, a radioligand for quantitation of the dopamine transporter in the living brain using positron emission tomography. Synapse. 1996;22(4):386–90.

6. Ding YS, Fowler JS, Volkow ND, Gatley SJ, Logan J, Dewey SL, et al. Pharmacokinetics and in vivo specificity of [^{11}C]DL-threo-methylphenidate for the presynaptic dopaminergic neuron. Synapse. 1994;18(2):152–60.

7. Goodman MM, Kilts CD, Keil R, Shi B, Martarello L, Xing D, et al. 18F-labeled FECNT: a selective radioligand for PET imaging of brain dopamine transporters. Nucl Med Biol. 2000;27(1):1–12.

8. Fischman AJ, Bonab AA, Babich JW, Livni E, Alpert NM, Meltzer PC, et al. [^{11}C, ^{127}I] altropane: a highly selective ligand for PET imaging of dopamine transporter sites. Synapse. 2001;39(4):332–42.

9. Emond P, Garreau L, Chalon S, Boazi M, Caillet M, Bricard J, et al. Synthesis and ligand binding of nortropane derivatives: N-substituted 2beta-carbomethoxy-3beta-(4'-iodophenyl)nortropane and N-(3-iodoprop-(2E)-enyl)-2beta-carbomethoxy-3beta-(3',4'-disubstituted phenyl)nortropane. New high-affinity and selective compounds for the dopamine transporter. J Med Chem. 1997;40(9):1366–72.

10. Chalon S, Hall H, Saba W, Garreau L, Dolle F, Halldin C, et al. Pharmacological characterization of (E)-N-(4-fluorobut-2-enyl)-2beta-carbomethoxy-3beta-(4'-tolyl)nortropane (LBT-999) as a highly promising fluorinated ligand for the dopamine transporter. J Pharmacol Exp Ther. 2006;317(1):147–52.

11. Halldin C, Erixon-Lindroth N, Pauli S, Chou YH, Okubo Y, Karlsson P, et al. [^{11}C]PE2I: a highly selective radioligand for PET examination of the dopamine transporter in monkey and human brain. Eur J Nucl Med Mol Imaging. 2003;30(9):1220–30.

12. Leroy C, Comtat C, Trebossen R, Syrota A, Martinot JL, Ribeiro MJ. Assessment of ^{11}C-PE2I binding to the neuronal dopamine transporter in humans with the high-spatial-resolution PET scanner HRRT. J Nucl Med. 2007;48(4):538–46.

13. Prunier C, Bezard E, Montharu J, Mantzarides M, Besnard JC, Baulieu JL, et al. Presymptomatic diagnosis of experimental Parkinsonism with ^{123}I-PE2I SPECT. Neuroimage. 2003;19(3):810–6.

14. Prunier C, Payoux P, Guilloteau D, Chalon S, Giraudeau B, Majorel C, et al. Quantification of dopamine transporter by ^{123}I-PE2I SPECT and the noninvasive Logan graphical method in Parkinson's disease. J Nucl Med. 2003;44(5):663–70.

15. Jucaite A, Fernell E, Halldin C, Forssberg H, Farde L. Reduced midbrain dopamine transporter binding in male adolescents with attention-deficit/hyperactivity disorder: association between striatal dopamine markers and motor hyperactivity. Biol Psychiatry. 2005;57(3):229–38.

16. Poyot T, Conde F, Gregoire MC, Frouin V, Coulon C, Fuseau C, et al. Anatomic and biochemical correlates of the dopamine transporter ligand ^{11}C-PE2I in normal and Parkinsonian primates: comparison with 6-[^{18}F]fluoro-L-dopa. J Cereb Blood Flow Metab. 2001;21(7):782–92.

17. Arakawa R, Ichimiya T, Ito H, Takano A, Okumura M, Takahashi H, et al. Increase in thalamic binding of [^{11}C]PE2I in patients with schizophrenia: a positron emission tomography study of dopamine transporter. J Psychiatr Res. 2009;43(15):1219–23.

18. Pinborg LH, Videbaek C, Svarer C, Yndgaard S, Paulson OB, Knudsen GM. Quantification of [^{123}I]PE2I binding to dopamine transporters with SPET. Eur J Nucl Med Mol Imaging. 2002;29(5):623–31.

19. Pinborg LH, Ziebell M, Frokjaer VG, de Nijs R, Svarer C, Haugbol S, et al. Quantification of ^{123}I-PE2I binding to dopamine transporter with SPECT after bolus and bolus/infusion. J Nucl Med. 2005;46(7):1119–27.

20. Delorenzo C, Kumar JD, Zanderigo F, Mann JJ, Parsey RV. Modeling considerations for in vivo quantification of the dopamine transporter using [^{11}C]PE2I and positron emission tomography. J Cereb Blood Flow Metab. 2009;29(7):1332–45.

21. Hirvonen J, Johansson J, Teras M, Oikonen V, Lumme V, Virsu P, et al. Measurement of striatal and extrastriatal dopamine transporter binding with high-resolution PET and [^{11}C]PE2I: quantitative modeling and test–retest reproducibility. J Cereb Blood Flow Metab. 2008;28(5):1059–69.

22. Jucaite A, Odano I, Olsson H, Pauli S, Halldin C, Farde L. Quantitative analyses of regional [^{11}C]PE2I binding to the dopamine transporter in the human brain: a PET study. Eur J Nucl Med Mol Imaging. 2006;33(6):657–68.

23. Lammertsma AA, Hume SP. Simplified reference tissue model for PET receptor studies. Neuroimage. 1996;4(3 Pt 1):153–8.

24. Ichise M, Ballinger JR, Golan H, Vines D, Luong A, Tsai S, et al. Noninvasive quantification of dopamine D2 receptors with iodine-123-IBF SPECT. J Nucl Med. 1996;37(3):513–20.

25. Huang SC, Barrio JR, Phelps ME. Neuroreceptor assay with positron emission tomography: equilibrium versus dynamic approaches. J Cereb Blood Flow Metab. 1986;6(5):515–21.

26. Innis RB, Cunningham VJ, Delforge J, Fujita M, Gjedde A, Gunn RN, et al. Consensus nomenclature for in vivo imaging of reversibly binding radioligands. J Cereb Blood Flow Metab. 2007;27(9):1533–9.

27. Mintum MA, Raichle ME, Kilbourn MR, Wooten GL, Welch MJ. A quantitative model for the in vivo assessment of drug binding sites with positron emission tomography. Ann Neurol. 1984;15:217–27.

28. Akaike H. A new look at the statistical model identification. IEEE Trans Automat Control. 1974;19:716–23.

29. Logan J, Fowler JS, Volkow ND, Wolf AP, Dewey SL, Schlyer DJ, et al. Graphical analysis of reversible radioligand binding from time–activity measurements applied to [N-^{11}C-methyl]-(−)-cocaine PET studies in human subjects. J Cereb Blood Flow Metab. 1990;10(5):740–7.

30. Hurley MJ, Mash DC, Jenner P. Markers for dopaminergic neurotransmission in the cerebellum in normal individuals and patients with Parkinson's disease examined by RT-PCR. Eur J Neurosci. 2003;18(9):2668–72.

31. Suzuki K, Sasaki M, Kubodera A. Approach to ultra high specific activity for 11C-labeled compounds. Synthesis of [11C]FLB 457 and [11C]Ro-15-4513. J Labelled Comp Radiopharm. 1999;42:S129–31.

32. Suzuki K, Inoue O, Tamate K, Mikado F. Production of 3-N-[^{11}C]methylspiperone with high specific activity and high radiochemical purity for PET studies: suppression of its radiolysis. Int J Rad Appl Instrum A. 1990;41(6):593–9.

33. Brix G, Zaers J, LE Adam, Bellemann ME, Ostertag H, Trojan H, et al. Performance evaluation of a whole-body PET scanner using the NEMA protocol. National Electrical Manufacturers Association. J Nucl Med. 1997;38(10):1614–23.

34. Eriksson L, Holte S, Bohm C, Kesselberg M, Hovander B. Automated blood sampling system for positron emission tomography. IEEE Trans Nucl Sci. 1988;35:703–7.

35. Friston KJ, Holmes AP, Poline JB, Grasby PJ, Williams SC, Frackowiak RS, et al. Analysis of fMRI time-series revisited. Neuroimage. 1995;2(1):45–53.

36. Hall H, Halldin C, Guilloteau D, Chalon S, Emond P, Besnard J, et al. Visualization of the dopamine transporter in the human brain postmortem with the new selective ligand [^{125}I]PE2I. Neuroimage. 1999;9(1):108–16.

Springer

37. Shetty HU, Zoghbi SS, Liow JS, Ichise M, Hong J, Musachio JL, et al. Identification and regional distribution in rat brain of radiometabolites of the dopamine transporter PET radioligand [^{11}C]PE2I. Eur J Nucl Med Mol Imaging. 2007;34(5):667–78.

38. Slifstein M, Laruelle M. Effects of statistical noise on graphic analysis of PET neuroreceptor studies. J Nucl Med. 2000;41(12):2083–8.

39. Parsey RV, Slifstein M, Hwang DR, Abi-Dargham A, Simpson N, Mawlawi O, et al. Validation and reproducibility of measurement of 5-HT1A receptor parameters with [carbonyl-^{11}C]WAY-100635 in humans: comparison of arterial and reference tissue input functions. J Cereb Blood Flow Metab. 2000;20(7):1111–33.

40. Ichise M, Liow JS, Lu JQ, Takano A, Model K, Toyama H, et al. Linearized reference tissue parametric imaging methods: application to [^{11}C]DASB positron emission tomography studies of the serotonin transporter in human brain. J Cereb Blood Flow Metab. 2003;23(9):1096–112.

Contents lists available at ScienceDirect

Life Sciences

Decreased binding of [11C]NNC112 and [11C]SCH23390 in patients with chronic schizophrenia

Jun Kosaka [a,b], Hidehiko Takahashi [a], Hiroshi Ito [a], Akihiro Takano [a], Yota Fujimura [a], Ryohei Matsumoto [a], Shoko Nozaki [a], Fumihiko Yasuno [a], Yoshiro Okubo [c], Toshifumi Kishimoto [b], Tetsuya Suhara [a,*]

[a] Molecular Neuroimaging Group, Molecular Imaging Center, National Institute of Radiological Sciences, 4-9-1 Anagawa, Inage-ku, Chiba 263-8555, Japan
[b] Department of Psychiatry, Nara Medical University, 840, Shijo-cho, Kashihara-shi, Nara 634-8521, Japan
[c] Department of Neuropsychiatry, Nippon Medical School, 1-1-5 Sendagi, Bunkyo-ku, Tokyo 113-8602, Japan

ARTICLE INFO

ABSTRACT

Aims: Abnormality of cognitive function in schizophrenia has been suggested to be related to dopamine D_1 receptor. However, the results of previous positron emission tomography (PET) studies of dopamine D_1 receptor in schizophrenia were not consistent.
Main methods: In this study, six patients with schizophrenia in severe residual phase with chronic antipsychotic treatment and twelve healthy age-matched controls participated. Two different radioligands, [11C]NNC112 and [11C]SCH23390, for dopamine D_1 receptor were used on the same subjects. Binding of the ligands was measured by PET, and statistical analysis was performed using one-way analysis of covariate (ANCOVA) with age as covariate.
Key findings: Good correlations between binding potential values (BP_{ND}) and age were observed in all regions of interest (ROIs) with both ligands. ANCOVA with age as covariate of BP_{ND} values of all ROIs revealed that the patient group showed significantly lower BP_{ND} value compared with the control group in both ligands.
Significance: In patients with chronic schizophrenia in severe residual phase with chronic antipsychotic treatment, the binding potential values of both ligands were significantly lower in the striatum and cortical regions than those of healthy controls.

© 2010 Elsevier Inc. All rights reserved.

Introduction

Schizophrenia is a chronic illness characterized by positive, negative, cognitive and affective symptoms (Schultz and Andreasen 1999). Although a positive symptom is characteristic of schizophrenia in the acute phase, the characteristic symptoms in the severe residual phase are negative symptom and cognitive dysfunction. The dopamine hypothesis is widely accepted for the pathophysiology of schizophrenia. Regarding dopamine receptors, the density of dopamine D_1 receptor in the cortical region is several times higher than that of dopamine D_2 receptor (Lidow et al. 1998). Abnormality of cognitive function in schizophrenia has been suggested to be related to dopamine function in the prefrontal cortex (Sawaguchi and Goldman-Rakic 1991). Dopamine D_1 receptor plays important roles in cognitive function such as working memory (Goldman-Rakic, 2000). One postmortem study has reported low dopamine D_1 receptors in the striatum in patients with schizophrenia (Hess et al. 1987), but no significant change has been reported in other studies (Seeman et al. 1987; Czudek and Reynolds 1988; Knable et al. 1994). In vivo PET studies reported decreased (Okubo et al. 1997),

unaltered (Karlsson et al. 2002), and increased (Abi-Dargham et al. 2002) binding of D_1 receptor in patients with schizophrenia compared with control subjects. Those results were possibly influenced by parameters of the particular patient populations including duration of illness, symptoms and medications. In addition, differences in radioligand [11C]SCH23390 (Okubo et al. 1997; Karlsson et al. 2002) and [11C]NNC112 (Abi-Dargham et al. 2002) were suggested to account for inconsistent PET findings. Furthermore, subjects were medication-free or -naïve patients with schizophrenia in the prodromal, acute or active phase, and the duration of untreated illness may have influenced the difference in dopamine D_1 receptor binding in previous human PET studies.

The purpose of the present study was to compare the dopamine D_1 receptor binding of chronic patients with schizophrenia in severe residual phase with chronic antipsychotic treatment to that of healthy controls in the striatum and extrastriatal regions using both [11C]SCH23390 and [11C]NNC112 in the same subjects.

Materials and methods

Subjects

Six patients with schizophrenia, 1 female and 5 males aged 46.5 ± 8.2 years (mean ± SD), participated in this study (Table 1). All patients

* Corresponding author. Tel.: +81 43 206 3251; fax: +81 43 253 0396.
E-mail address: suhara@nirs.go.jp (T. Suhara).